Journal of Energy Storage 96 (2024) 112732

Contents lists available at ScienceDirect

Journal of Energy Storage

journal homepage: www.elsevier.com/locate/est

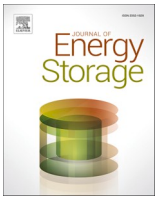

Research Papers

Design and optimization of a cascade hydrogen storage system for integrated energy utilization

Shihao Zhu [a], Banghua Du [b,*], Xinyu Lu [a], Changjun Xie [a,b,**], Yang Li [c], Yunhui Huang [a], Leiqi Zhang [d], Bo Zhao [d]

[a] School of Automation, Wuhan University of Technology, Wuhan 430070, China
[b] Hubei Key Laboratory of Advanced Technology for Automotive Components, Wuhan University of Technology, Wuhan 430070, China
[c] Department of Electrical Engineering, Chalmers University of Technology, Gothenburg 41258, Sweden
[d] State Grid Zhejiang Electric Power Research Institute, Hangzhou 310014, China

ARTICLE INFO

Keywords:
Hydrogen storage system
Multipath
Integrated hydrogen energy utilization system

ABSTRACT

In an integrated hydrogen energy utilization system, the hydrogen storage device needs to meet hydrogen supplies and demands of different pressure levels, traditional hydrogen storage systems will lead to more energy consumption and lower hydrogen supply efficiency. To address this problem, a cascade hydrogen storage system (CHSS) is proposed in this study. By configuring three hydrogen storage tanks (HSTs) with three pressure levels, the CHSS is capable of serving hydrogen for fuel cell supply, long-term storage, and refueling stations. The corresponding control strategy of hydrogen flow between HSTs is proposed. It shows that an optimal capacity configuration scheme with pressures of 3 MPa, 24.44 MPa, and 45 MPa and a hydrogen storage capacity of 401.7 kg, optimized by NSGA-II, can meet the stable operation of the system. Comparative studies show that the proposed CHSS configuration can reduce the cost by about 3.78 %, the energy consumption by about 6.92 %, and the hydrogen supply loss rate by about 12 % compared to the existing solutions under the tested conditions.

1. Introduction

As the most promising alternative to fossil fuels, hydrogen has demonstrated advantages such as non-pollution and high energy density [1,2]. It can be obtained from various sources, including water electrolysis and the synthesis of industrial by-products [3,4]. As a sustainable energy source, hydrogen can play a crucial role in the future energy system to mitigate the power fluctuations in renewable generation [5]. The implementation of a hydrogen storage system (HSS) is essential to facilitate effective hydrogen utilization, ensuring efficient storage and transportation of this clean energy carrier. Nevertheless, the current HSS encounters challenges such as high costs and low energy conversion efficiency, impeding its overall development. For example, Abdin [6] et al. argues that the long-term storage cost of hydrogen far exceeds the generation cost. Elberry [7] et al. pointed that the low specific gravity of hydrogen leads to the challenge of high energy density for hydrogen storage, which is not conducive to improving the efficiency of hydrogen storage systems. Therefore, there is an urgent need to enhance the energy efficiency and cost-effectiveness of the HSS to encourage widespread hydrogen utilization on a large scale.

There are two main categories of viable technical solutions for hydrogen storage. The first involves physical storage systems, including room-temperature compressed gas hydrogen storage (CGH_2) and liquid hydrogen storage (LH_2) technology, among others [8,9]. The second category comprises material-based storage systems, such as adsorption hydrogen storage and metal hydrides (MH) [10]. LH_2 can achieve superior energy storage densities compared to compressed gas. However, the liquefaction process demands the consumption of >30 % of the hydrogen combustion energy [11,12]. The hydrogen adsorption capacity of porous materials has been reported to be <1 % at ambient temperature and pressure [13]. MH exhibits greater hydrogen binding ability, albeit requiring release at high temperatures or low external pressures [14]. Upon comparing the above technologies, CGH_2 emerges with the advantages of high energy density, ease of storage, and lower power consumption [15–17]. Consequently, it is considered the prevailing technology widely employed in practical engineering applications.

In contrast to single-energy renewable energy systems, the integration of hydrogen energy in a hydrogen-electric coupling system (HECS)

* Corresponding author.
** Correspondence to: C. Xie, School of Automation, Wuhan University of Technology, Wuhan 430070, China.
E-mail addresses: dubanghua@whut.edu.cn (B. Du), jackxie@whut.edu.cn (C. Xie).

https://doi.org/10.1016/j.est.2024.112732
Received 2 March 2024; Received in revised form 17 June 2024; Accepted 20 June 2024
Available online 28 June 2024
2352-152X/© 2024 Elsevier Ltd. All rights are reserved, including those for text and data mining, AI training, and similar technologies.

Nomenclature

Subscripts and superscripts

HST	Hydrogen storage tank
0	Initial state
EL	Electrolyzer
FC	Fuel cell
HRS	Hydrogen refueling station
L	Low-pressure HST
M	Medium-pressure HST
H	High-pressure HST
com	Compressor
p	Constant pressure
in	Inlet
out	Outlet
HV	Hydrogen fuel cell vehicle
inv	Investment
o&m	Operation and maintenance
aux	Auxiliary equipment
CHSS	Cascade hydrogen storage system

Symbols

N	Amount of substance, mol
M	Molar mass, g/mol
F	Molar flow rate, mol/s
P	Power, W
C	Specific heat capacity, J/(mol K)
T	Temperature, K
p	Pressure, Pa
w	Weight, dimensionless
R	Rank, dimensionless

Greek symbols

η	Efficiency
γ	Adiabatic coefficient

Abbreviations

HSS	Hydrogen storage system
CGH_2	Compressed gas hydrogen storage
LH_2	Liquid hydrogen storage
MH	Metal hydrides
HECS	Hydrogen-electric coupling system
PV	Photovoltaic
IES	Integrated energy system
HST	Hydrogen storage tank
FC	Fuel cell
HRS	Hydrogen refueling station
EL	Electrolyzer
CHSS	Cascade hydrogen storage system
IHEUS	Integrated hydrogen energy utilization system
NSGA	Non-dominated sorting genetic algorithm
SHSS	Single-stage hydrogen storage system
LHST/MHST/HHST	Low-/medium-/high-pressure HST
SOH	State of hydrogen storage
HSLR	Hydrogen supply loss rate

has been shown to significantly improve the system performance for extended operating cycles [18], and much effort has been devoted to designing modern HECSs. For example, Maghami et al. [19] proposed an HECS for synchronized energy output by developing a program logic controller unit for energy management, considering a demand response program. Basu et al. [20] studied three different forms of energy systems. Through the results of HOMER simulations, it was concluded that the solar-wind-hydrogen hybrid system demonstrated the most cost-effective. Song et al. [21] proposed an HECS that utilizes surplus electricity to produce hydrogen, which provides a solution for small public buildings to solve the problem of photovoltaic (PV) power curtailment. Abdin et al. [22] investigated the minimum cost of energy in five cities in Canada, the United States, and Australia. They used the multiple energy optimization model in the microgrid simulation software HOMER Pro to obtain the optimal sizing of system components. A refined model was developed along with a proposed synergistic configuration of an electric-hydrogen-heat-gas integrated energy system (EHTG-IES), which can reduce the costs and the carbon emissions by 3.18 % and 5.05 %, respectively [23]. The studies mentioned above emphasize the enhancement of HECS performance compared to single electrical energy systems, with a lack of research concerning the structure and performance of HSSs.

Regarding the structure of the HSS, Li et al. [24] studied the effect of the initial filling pressure of hydrogen storage tanks (HSTs) with different pressures on the rapid refueling of hydrogen fuel cell (FC) vehicles. They confirmed that the increase of the initial pressure of refueling can effectively reduce the final temperature at the time of the completion of refueling. Tarhan et al. [25] explored various approaches to designing HSSs and highlighted that underground hydrogen storage is an effective approach for Romania. The method offers advantages, including a simple and fast process for both filling and draining. Mayer et al. [26] proposed a cascade high-pressure hydrogen storage device for hydrogen refueling stations (HRSs), where the volume of HSTs and the maximum pressure were optimized to minimize the lifecycle costs. Fragiacomo et al. [27] proposed an energy analysis method for hydrogen production and storage systems to investigate the effect of the pressure level of the high-pressure HSS on the hydrogen refueling rate for hydrogen production in an electrolyzer (EL). The above studies are limited to HSSs with a single pressure level, with no simultaneous consideration of the production and utilization phases. Additionally, there is no comparison made between multiple pressure levels and a single pressure level. This is not conducive to optimizing the performance of HSSs.

For capacity allocation optimization, Ahmadi et al. [28] introduced a decentralized two-energy stochastic optimization method. This approach relies on an asymptotic hedging algorithm designed for multi-energy microgrids with multi-intelligent systems. The goal is to improve the stability of hybrid energy storage microgrids. Hu et al. [29] proposed an energy allocation optimization method for HECS using multimode control. In order to reduce the degradation of the battery capacity and energy loss, the optimized weight coefficients were allocated and the upper limit of battery charging and discharging power were optimized by using the gray wolf optimization algorithm. Zhang et al. [5] minimized the energy cost of hydrogen-based energy hubs for integrated demand response and HSSs using harmony search algorithms. Xu et al. [30] presented a data-driven two-stage multi-criteria decision-making framework applied to optimize the configuration of stand-alone wind/photovoltaic/hydrogen systems. They validated the effectiveness of their optimization results by implementing the algorithm for an industrial park located in Gansu Province. Pan et al. [31] proposed a hybrid planning model for an electric-hydrogen-integrated energy system by combining stochastic optimization and robust optimization, solved by nested columns and constraint generation algorithms. The studies mentioned above are aimed at exploring more rational energy system configurations without addressing the capacity configuration of HSSs.

Indeed, the HSS serves as a crucial energy storage unit for hydrogen energy systems. Designing a system that balances both economy and efficiency is important for enhancing the performance of HECSs, but

unfortunately, relevant studies are rare at the moment. Therefore, this study proposes a cascade hydrogen storage system (CHSS) suitable for an integrated hydrogen energy utilization system (IHEUS). The system undertakes the functions of hydrogen supply to FCs, long-term hydrogen storage, and hydrogen supply to HRSs through three HSTs with different pressure levels. Auxiliary supporting control strategies enable synergistic work between all levels of HST to improve system efficiency. The proposed CHSS is compared with the conventional single-stage system, and the optimal capacity configuration is optimized based on the non-dominated sorting genetic algorithm II (NSGA-II). Finally, the feasibility and economy of the CHSS are verified by considering real operating conditions for operational tests. The main work and contributions of this study are as follows:

1) A CHSS for IHEUS is proposed. The hydrogen produced by the hydrogen production system is stored in three tanks with different pressure levels, which are used for supplying hydrogen to the power generation system, long-term storage of hydrogen and supplying hydrogen to the HRS, respectively. The corresponding hydrogen management strategy is also designed to improve the stability of the system.
2) By establishing the mathematical model and economic model of the HSS, the NSGA-II is used to optimize the system capacity configuration, and the optimal CHSS configuration results are obtained by weighted calculation combined with the engineering practice.
3) The CHSS is compared and analyzed with the single-stage HSS (SHSS), and the economy of the MHSS is verified, which provides a theoretical basis for the design of the HSS structure. The stability and economy of the system are also verified under the off-grid condition of 168 h.

The rest of the paper is organized as follows. Section 2 presents the detailed structure of the CHSS proposed in this study and briefly derives the simulation model. Section 3 proposes the control strategy of the system and establishes the multi-objective function of the CHSS with corresponding constraints. Section 4 obtains the optimal capacity allocation results, verifies the economics of the CHSS compared with the conventional SHSS, and tests the stability and economics of the system under off-grid short-term operation. Conclusions are obtained in Section 5.

2. System description and development

A conventional IHEUS with SHSS typically comprises four components: A hydrogen production system (PEMEL), a HSS with several identical HSTs, a power generation system (PEMFC), and an HRS, as shown in Fig. 1(a). The hydrogen generated by the PEMEL is sequentially fed into the HSTs through a multi-way valve and then used to supply the FC and HRS. If the pressure in the HSTs is higher than that in the PEMEL, the pressure needs to be increased to the rated pressure before a filling process. On the other hand, if the HSTs' pressure is lower than that required for hydrogen refueling at the HRS, the hydrogen in the HSTs needs to be pressurized to match the station's demand before delivering the hydrogen.

In order to improve the flexibility and economy of hydrogen storage, this study proposes to design a CHSS scheme for IHEUS. In contrast to the conventional scheme, in our proposed design with a CHSS as shown in Fig. 1(b), the hydrogen generated by the EL is first fed into a low-pressure HST (LHST). The hydrogen in the LHST can be directly utilized by the FC or delivered to a medium-pressure HST (MHST). If the pressure in the MHST is lower than that in the LHST, the hydrogen can be directly transferred through a pipeline. If the pressure in the MHST is higher than that in the LHST, the hydrogen needs to be pressurized using a compressor before delivery. A second compressor further raises the pressure, and the processed hydrogen is stored in a high-pressure HST (HHST). In this new scheme, the LHST serves as the buffer stage, which is responsible for delivering hydrogen to the PEMFC, while the HHST only serves as the hydrogen source to the HRS.

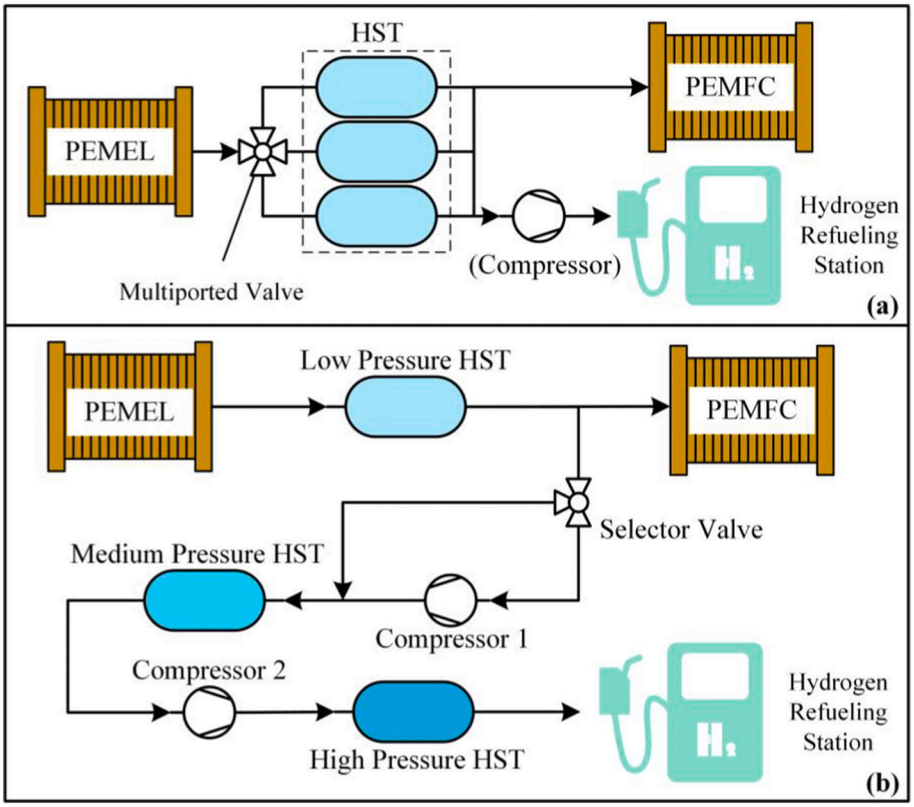

Fig. 1. Schematic diagram of (a) the conventional IHEUS with SHSS and (b) the proposed IHEUS with CHSS.

2.1. Hydrogen storage tank

The HSTs in the HSS use CGH_2 technology to absorb the hydrogen produced by the PEMEL and deliver the hydrogen when it is needed by the FC or HRS. In Fig. 1(a), the state of hydrogen storage (SOH) is defined to measure the total amount of hydrogen stored in all tanks, calculated by [32].

$$\begin{aligned}\mathrm{SOH} &= \frac{N_{\mathrm{HST}}}{M_{\mathrm{H_2}}} \\ &= \mathrm{SOH}_0 + \frac{1}{M_{\mathrm{H_2}}}\int_0^t \left(\underbrace{F_{\mathrm{H_2,\ EL}}}_{\substack{\text{Output } H_2 \text{ molar}\\ \text{flow rate of EL}}} - \underbrace{F_{\mathrm{H_2,\ FC}}}_{\substack{\text{Input } H_2 \text{ molar}\\ \text{flow rate of FC}}} - \underbrace{F_{\mathrm{H_2,HRS}}}_{\substack{\text{Input } H_2 \text{ molar}\\ \text{flow rate of HRS}}} \right) dt \end{aligned} \tag{1}$$

where N_{HST} is the amount of hydrogen stored in the HST, $M_{\mathrm{H_2}}$ is the molar mass of hydrogen ($M_{\mathrm{H_2}} = 2$ g/mol), and SOH_0 is the initial hydrogen mass. In contrast, in the proposed design with CHSS, the SOH needs to be defined individually for each HST, given by

$$\begin{cases} \mathrm{SOH}_L = \mathrm{SOH}_{L0} + \dfrac{1}{M_{\mathrm{H_2}}}\displaystyle\int_0^t \left(\underbrace{F_{\mathrm{H_2,\ EL}}}_{\text{Output } H_2 \text{ molar flow rate of EL}} - \underbrace{F_{\mathrm{H_2,\ FC}}}_{\text{Input } H_2 \text{ molar flow rate of FC}} - \underbrace{F_{\mathrm{H_2,com1}}}_{\text{Input } H_2 \text{ molar flow rate of MHST}} \right) dt \\ \mathrm{SOH}_M = \mathrm{SOH}_{M0} + \dfrac{1}{M_{\mathrm{H_2}}}\displaystyle\int_0^t \left(\underbrace{F_{\mathrm{H_2,com1}}}_{\text{Output } H_2 \text{ molar flow rate of LHST}} - \underbrace{F_{\mathrm{H_2,com2}}}_{\text{Input } H_2 \text{ molar flow rate of HHST}} \right) dt \\ \mathrm{SOH}_H = \mathrm{SOH}_{H0} + \dfrac{1}{M_{\mathrm{H_2}}}\displaystyle\int_0^t \left(\underbrace{F_{\mathrm{H_2,com2}}}_{\text{Output } H_2 \text{ molar flow rate of MHST}} - \underbrace{F_{\mathrm{H_2,HRS}}}_{\text{Input } H_2 \text{ molar flow rate of HRS}} \right) dt \end{cases} \tag{2}$$

where SOH_{L0}, SOH_{M0}, and SOH_{H0} are the initial hydrogen storage masses of the low-, medium-, and high-pressure HST, respectively.

2.2. Hydrogen compressor

A hydrogen compressor is used to pressurize the hydrogen from a lower- to a higher-pressure level. The power is consumed in an isentropic compression process, given by [33].

$$P_{\mathrm{com}} = \frac{F_{\mathrm{H_2}} C_{p,\mathrm{H_2}} T}{\eta_{\mathrm{com}}} \left[\left(\frac{p_{\mathrm{out}}}{p_{\mathrm{in}}} \right)^{\frac{\gamma-1}{\gamma}} - 1 \right] \tag{3}$$

where $F_{\mathrm{H_2}}$ is the molar flow rate of hydrogen, $C_{p,\mathrm{H_2}}$ is the specific heat capacity of hydrogen at constant pressure (14.3 J/mol•K), η_{com} is the isentropic efficiency of the compressor, T is the temperature of the gas, γ is the adiabatic index of hydrogen (1.41, dimensionless), and p_{in} and p_{out} are the inlet and outlet pressures of the compressor, respectively.

3. Optimal control strategy

The required operating pressure for each subsystem of the IHEUS is given in Table 1 It can be seen that the pressure needed for the FC intake is much lower than the output pressure of hydrogen produced by the EL. In order to reduce the energy consumption during the compression process, the lower pressure limit of the HSS is set to 3 MPa, the same as that of EL. On the other hand, the HRS injects hydrogen gas at a pressure of 35 MPa, and according to regulations, the pressure level of the HST should be 45 MPa [34]. Therefore, the maximum pressure for the HST is set at 45 MPa.

We investigate three configuration schemes for the CHSS, denoted by Schemes 1 to 3, and the corresponding operating pressures are given in Table 2. In Scheme 2, the middle-level pressure, denoted by X, ranging from 3 to 45 MPa, needs to be determined to optimize the performance of the system. This will be discussed in latter sections.

3.1. Control strategy

In an SHSS, all HSTs in the HSS share the same priority during the scheduling process, and thus, the behaviors of all HSTs are consistent. In contrast, an individual control strategy needs to be designed for each HST in the proposed CHSS. The interaction between the CHSS and other devices in the IHEUS is illustrated in Fig. 2, where the direction of hydrogen flow in each process is indicated.

As mentioned eariler and also seen from Fig. 2, the FC only uses the LHST to receive the hydrogen produced by the EL, while the single hydrogen supply for the HRS is the HHST. Furthermore, once the pressure of an HST reaches its upper limit, its hydrogen will be delivered to the HST with higher operating pressure. On the other hand, when the pressure becomes too low due to the lack of hydrogen storage, the corresponding HST can be replenished from the lower-level tank. If both LHST and MHST hydrogen reaches the lower capacity limit, the LHST would receive hydrogen from the HHST directly. Based on the principles, control rules of CHSS are designed and depicted as an flow chart in Fig. 3.

As can be seen from Fig. 3, when the EL working state is ON ($S_{\mathrm{EL}} = 1$), the EL starts to deliver hydrogen to the LHST. When the FC's working state is ON ($S_{\mathrm{FC}} = 1$), the FC starts to receive hydrogen from the LHST. When an FC vehicle enters the HRS ($S_{\mathrm{HV}} = 1$), the hydrogen refueler starts to receive hydrogen from the HHST. The CESS working state is determined according to the HST pressure as follows:

Table 1
Hydrogen pressure for different devices.

Device	Hydrogen input/output pressure (MPa)
PEMEL	3
PEMFC	0.6
HRS	35

Table 2
Proposed hydrogen storage scheme.

Scheme	Hydrogen storage pressure (MPa)
1	3 + 3 + 3
2	3 + X + 45
3	45 + 45 + 45

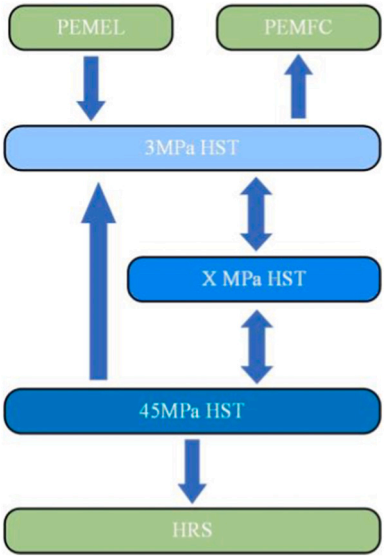

Fig. 2. Schematic diagram of CHSS.

1) When the pressure sensor of LHST detects that its pressure drops to 0.6 MPa, and the PEMEL is not in operation at that time, the LHST sends a hydrogen demand signal to the system, and the hydrogen will be delivered from other HSTs to the LHST. If the pressure in the tank has reached 3 MPa, the LHST delivers its hydrogen to the MHST.
2) When the pressure sensor of MHST detects that its pressure is lower than 0.1 MPa (i.e., standard atmospheric pressure), the MHST sends a hydrogen demand signal to the system to avoid a vacuum state. At this point, the hydrogen will be delivered from the other HST to the MHST. If the pressure inside the tank reaches X MPa, the MHST will deliver its hydrogen to the HHST.
3) When the pressure sensor of HHST detects that the pressure in the tank is below 35 MPa, the HHST sends a hydrogen demand signal to the system, and then the hydrogen will be delivered from other HSTs to the HHST. If the tank pressure reaches 45 MPa, the HHST will stop receiving hydrogen.

3.2. Objective functions and constraints

After determining the control strategy of the CESS, it is necessary to select proper tank capacity for each HST to ensure the technical and economical viability. The specific objectives to be considered include the costs, power consumption of the compressors, and system capacity. We adopt a multi-objective optimization method to find the optimal configuration of the CESS and the procedure is described as follows.

First, the total costs C_{CHSS} of the CHSS is expressed as

$$C_{\mathrm{CHSS}} = C_{\mathrm{inv}} + C_{\mathrm{o\&m}} \tag{4}$$

where C_{inv} is the investment cost and $C_{\mathrm{o\&m}}$ is the operation and maintenance (O&M) cost. They are calculated by

$$\begin{cases} C_{\mathrm{inv}} = C_{\mathrm{L},0}\cdot V_{\mathrm{L}} + C_{\mathrm{M},0}\cdot V_{\mathrm{M}} + C_{\mathrm{H},0}\cdot V_{\mathrm{H}} + C_{\mathrm{aux}} \\ C_{\mathrm{o\&m}} = N_{life}\cdot\alpha\cdot C_{\mathrm{inv}} \end{cases} \tag{5}$$

where $C_{\mathrm{L},0}$, $C_{\mathrm{M},0}$, $C_{\mathrm{H},0}$, V_{L}, V_{M}, and V_{H} are the price per unit volume and hydrogen storage volumes of LHST, MHST, and HHST, respectively. C_{aux} is the cost of auxiliary equipment, including compressors, pipelines, valves and so on. According to market research, in this study, C_{aux} = 360,000 $ [35]. N_{life} is the operating life of IHEUS, which is typically 20 years [36], α is the O&M cost coefficient for the HST, which is typically 0.5 % [36].

The typical costs of the HSTs of different pressure levels are given in Table 3 [37]. Since these costs are given at specific pressure values, a linear function is used to fit the discrete data for later use, as shown in Fig. 4.

The CHSS capacity M_{MHSS} is defined as the maximum total hydrogen in terms of molar mass that can be stored in the three HSTs, i.e.,

$$M_{\mathrm{CHSS}} = m_{\mathrm{L}} + m_{\mathrm{M}} + m_{\mathrm{H}} \tag{6}$$

where m_{L}, m_{M}, and m_{H} are the upper SOH limits for LHST, MHST, and HHST, respectively.

The total power consumed by the two compressors of CHSS is closely related to the MHST pressure, which is calculated by

$$\begin{aligned} P_{\mathrm{com,CHSS}} &= \frac{F_{\mathrm{H_2}} C_{p,\mathrm{H_2}} T}{\eta_{\mathrm{com}}}\left[\left(\frac{p_{\mathrm{M}}}{3}\right)^{\frac{\gamma-1}{\gamma}} - 1\right] + \frac{F_{\mathrm{H_2}} C_{p,\mathrm{H_2}} T}{\eta_{\mathrm{com}}}\left[\left(\frac{45}{p_{\mathrm{M}}}\right)^{\frac{\gamma-1}{\gamma}} - 1\right] \\ &= \frac{F_{\mathrm{H_2}} C_{p,\mathrm{H_2}} T}{\eta_{\mathrm{com}}}\left[\left(\frac{X}{3}\right)^{\frac{\gamma-1}{\gamma}} - 1\right] + \frac{F_{\mathrm{H_2}} C_{p,\mathrm{H_2}} T}{\eta_{\mathrm{com}}}\left[\left(\frac{45}{X}\right)^{\frac{\gamma-1}{\gamma}} - 1\right] \end{aligned} \tag{7}$$

where $F_{\mathrm{H_2}}$ is the molar flow rate of hydrogen produced by EL injected into HHST, which is set to a value of 1 mol/s for the subsequent calculations, and p_{MHST} is the pressure magnitude of MHST, with its value being X.

According to the design requirements, the system needs to meet the hydrogen demands from at least one day to up to one week for off-grid operation. Therefore, the CHSS must independently supply the hydrogen $m_{\mathrm{H_2,IHEUS}}$ for at least one day of IHEUS, up to a maximum of seven days, i.e.,

$$m_{\mathrm{H_2,IHEUS}} \le M_{\mathrm{CHSS}} \le 7 m_{\mathrm{H_2,IHEUS}} \tag{8}$$

where, $m_{\mathrm{H_2,IHEUS}}$ is calculated based on actual condition and will be provided in Section 4.1.

In order to minimize the overall energy consumption, it is essential to reduce the usage of the hydrogen compressors. Compared to the frequent start-stop operation of compressors to maintain hydrogen levels in the HST, performing single hydrogen refilling sessions that keep the tank's hydrogen content at a higher level is more energy-efficient. This is because compressors consume significantly more energy during the startup phase [38]. Therefore, the LHST and HHST should independently fulfill the hydrogen demands of the PEMFC and HRS as frequently as possible, yielding the following constraints:

$$\begin{cases} m_{\mathrm{L}} \ge m_{\mathrm{H_2,FC}} \\ m_{\mathrm{H}} \ge m_{\mathrm{H_2,HRS}} \end{cases} \tag{9}$$

The objective function is

$$Minimizey = f(x) = \left[C_{\mathrm{CHSS}}(x), \frac{1}{M_{\mathrm{CHSS}}(x)}, P_{\mathrm{com,CHSS}}(x)\right] \tag{10}$$

subject to conditions (8), (9), and

$$3 \le p_{\mathrm{M}} \le 45 \tag{11}$$

where the decision vector x include m_{L}, m_{M}, m_{H} and p_{M}.

3.3. Methodology

A genetic algorithm (GA) is a stochastic search method inspired by genetics and the laws of natural selection [39]. GA can search a large part of the region, thus avoiding convergence to local extremes with high robustness. Therefore, GA is selected for solving multi-objective optimization problems. However, in the capacity allocation problem involved in this study, considering the tradeoff between the capacity size and the economic cost, the original GA is prone to receive the influence of the local optimal solution. Thus, the global optimal solution cannot be obtained. NSGA-II, as a variant of GA, was introduced to address this problem by adopting the elitism principle and the diversity preservation mechanism to obtain the Pareto optimal solution [40]. The elitism principle helps the algorithm to reduce the influence of local optimal

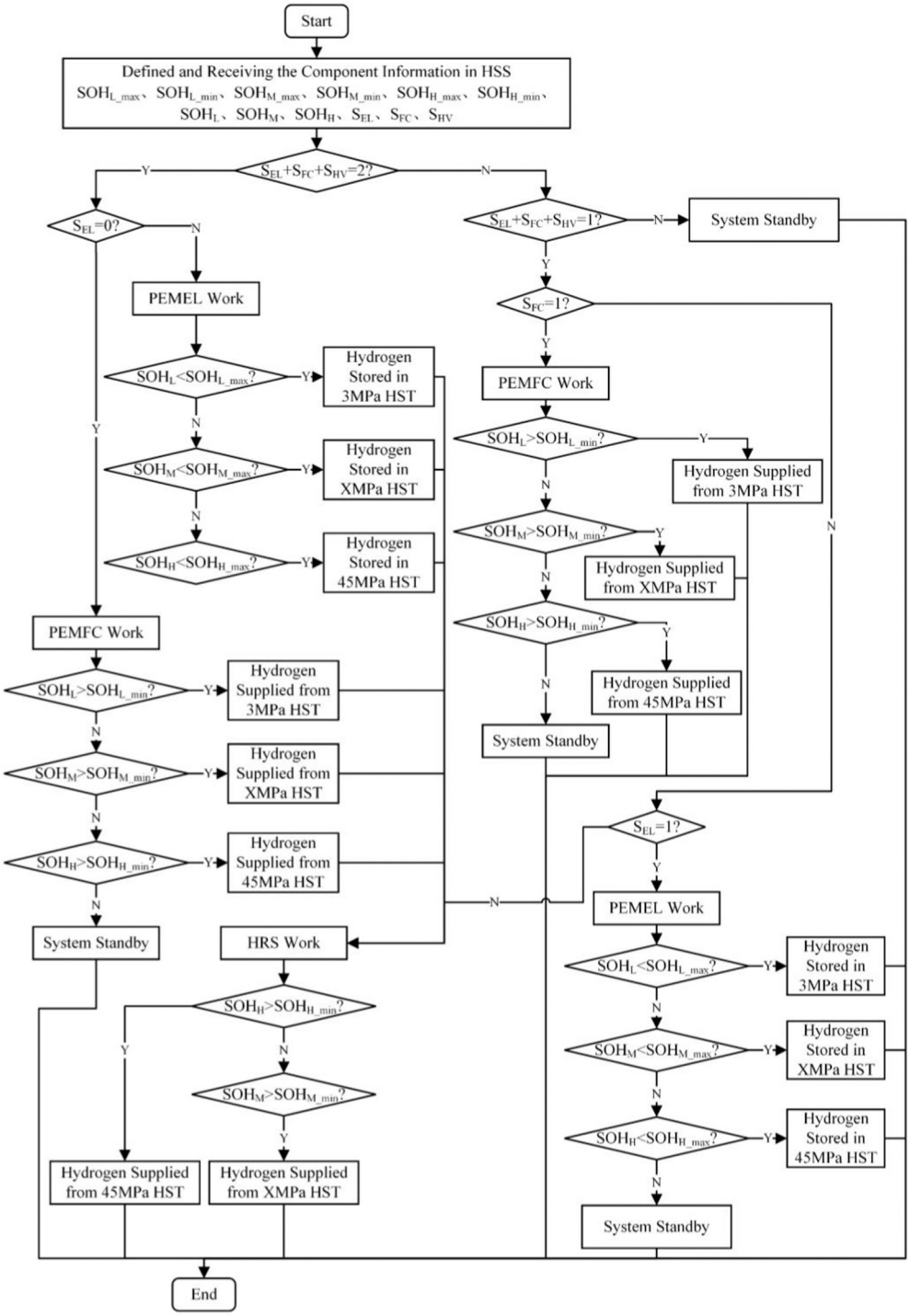

Fig. 3. Flowchart of CHSS control.

Table 3
Prices for HSTs of different pressures.

Pressure (MPa)	Unit price ($/m^3)
3	2000
10	8000
20	16,000
30	24,000
45	36,000

solutions of an objective function and thus converge to the global optimal solution. The diversity-preserving mechanism prevents the algorithm from converging too early and failing to explore the search space more comprehensively. In this study, the flow of NSGA-II is shown in Fig. 5.

4. Results and discussions

4.1. Case study

We chose a real-world demonstration project in Zhejiang Province,

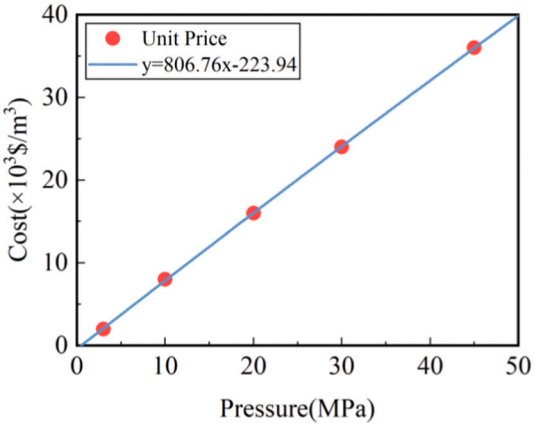

Fig. 4. HST pressure-price curve.

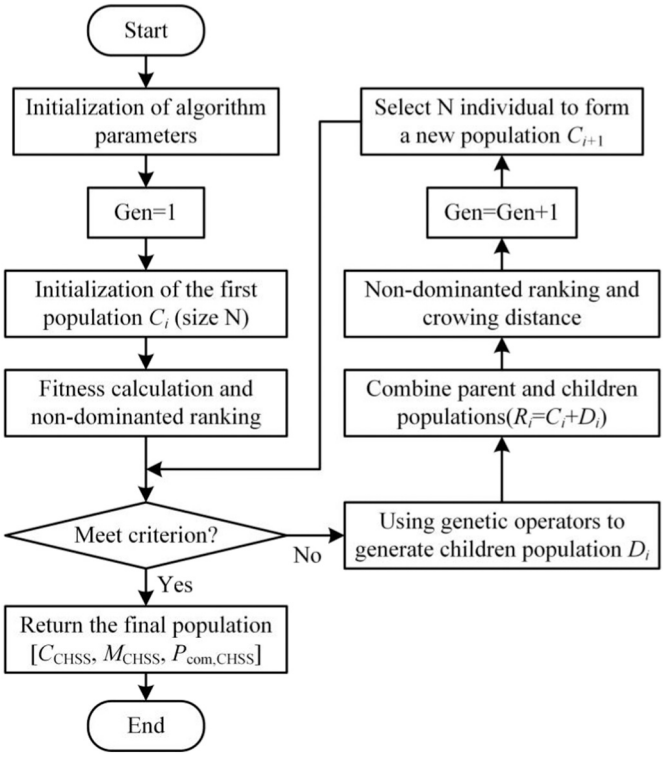

Fig. 5. Flowchart of NSGA-II.

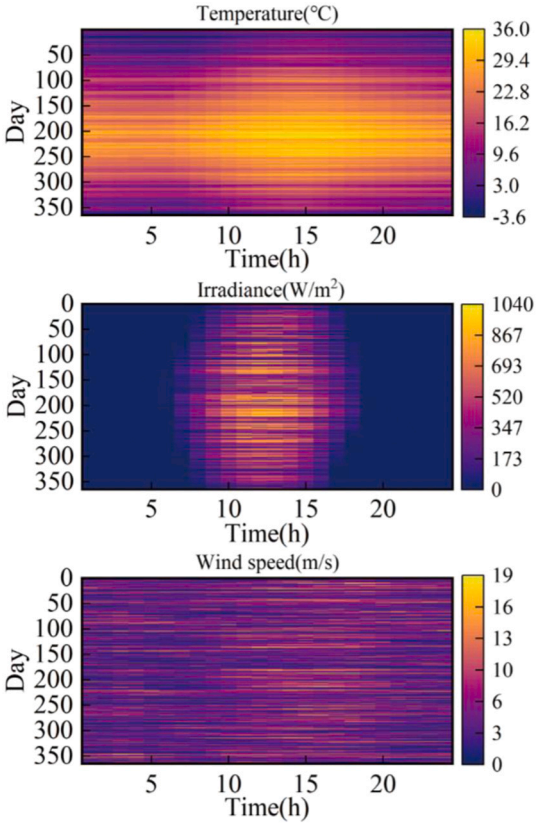

Fig. 6. Overall climatic conditions of the selected area.

Fig. 7. Demonstration park under investigation.

located in southeastern China, to demonstrate the effectiveness of the proposed design and optimization algorithm. The project is an industrial park along the coastal area. One-year field data of temperature, solar irradiance, and wind speed are collected from the local meteorological station, illustrated in Fig. 6.

Fig. 7 presents a photograph of the demonstration park under investigation. The specifications of the hydrogen production and consumption devices are given in Table 4. The microgrid within the demonstration park is connected to the utility grid under normal conditions. It is assumed that the PEMEL functions at its rated operating condition throughout the period when the microgrid is grid-connected, and the PEMFC is required to operate for two hours daily at the specified rated state. Furthermore, ten hydrogen FC vehicles are running in this area, with a variable number of vehicles, denoted as n ($0 \leq n \leq 10$), arriving at the designated refueling station during fixed intervals (13:00–14:00 and 21:00–22:00). Each vehicle refuels with 10 kg of hydrogen during these scheduled times.

Table 4
Device parameters.

Devices	Hydrogen production/consumption	Quantities
PEMEL	3.57 kg/h	2
PEMFC	7 kg/h	2
HRS	10 kg per vehicle	3

Based on the developed model in Section 2 and the control strategy in Section 3, and by applying the NSGA-II optimization method presented in Section 4, we obtain the optimal configuration of the HST capacity of each level of CHSS and the middle-level pressure X. Based on the data provided in Table 4 and the results of on-site surveys, we can determine that the PEMFC in the IHEUS operates in its rated state for an average of 2 h per day, and the hydrogen refueling station needs to meet the hydrogen demand for 10 hydrogen fuel cell vehicles. In summary, $m_{H_2,IHEUS}$ in Eq. (8) is 128 kg. Thus, the optimization results are

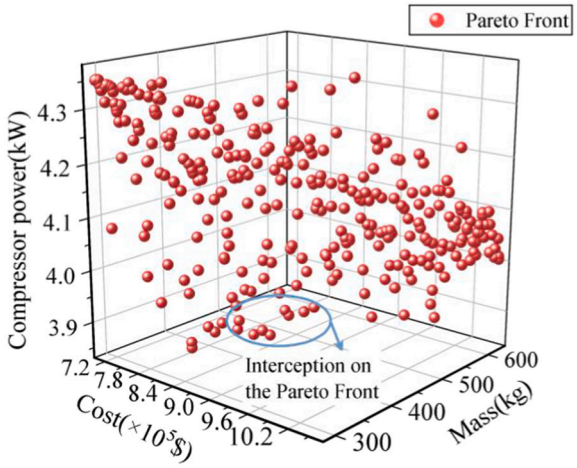

Fig. 8. Pareto Front for CHSS based on NSGA-II.

demonstrated in Figs. 8 and 9.

Cost, capacity, and power consumption are respectively taken as the x, y, and z axes. The population distribution obtained through NSGA-II optimization is shown in Fig. 8. Each point in the figure represents the objective function values corresponding to decision variables of the different population. From Fig. 8, it can be seen that the capacity is directly related to the cost of CHSS. According to Eq. (7), it is the pressure level of MHST the single factor that influences the energy consumption of the compressor unit, while the capacity of the HSTs does not affect its value. When optimizing the three variables, namely the cost, capacity, and energy consumption, the constraint relationship among them is not significant. Consequently, a higher-level compressor tends to consume more energy in order to achieve the minimum-cost operation, whereas the energy consumption of a lower-level compressor becomes more significant when capacity maximization is more emphasized. In a practical CHSS, a larger capacity, lower cost, and smaller energy consumption are expected. Therefore, a set of feasible solutions is tested in Fig. 8 to verify the performance of the optimized design.

Plotting the various decision variables from Fig. 8 as the y-values, with the population index as the x-axis, results in Fig. 9. From Fig. 9, it can be seen that the capacity of the LHST is concentrated within the range of 30 to 35 kg. This is because the LHST is primarily responsible for supplying hydrogen to the fuel cells rather than storing hydrogen for the long term. Most of the hydrogen produced by the hydrogen production system flows through the LHST to the MHST rather than remaining in the LHST. Choosing an excessively large capacity would only result in unnecessarily high costs and lead to overloaded hydrogen storage in the LHST, deviating from the design requirements. In addition, MHST presents the highest capacity because the MHST needs to fulfill the function of long-term hydrogen storage. If the LHST were used for long-term hydrogen storage, its lower storage pressure would require excessive space, which is not conducive to the system's construction. Conversely, if HHST is used for long-term hydrogen storage, its high storage pressure will require more energy for hydrogen compression. However, in the system, only the hydrogen refueling station needs high-pressure gas, and this portion of the gas is not the main component. Therefore, using HHST for hydrogen storage is less economical. Inadequate capacity of MHST can reduce the cost, but the long-term hydrogen storage requirement may fail to be met. The capacity of HHST is more evenly distributed. This is due to the fact that the capacity of HHST has less impact on energy consumption and is only related to the overall capacity of the CHSS, which is more evenly distributed in the search space to retrieve each situation. The pressure of the MHST is mainly

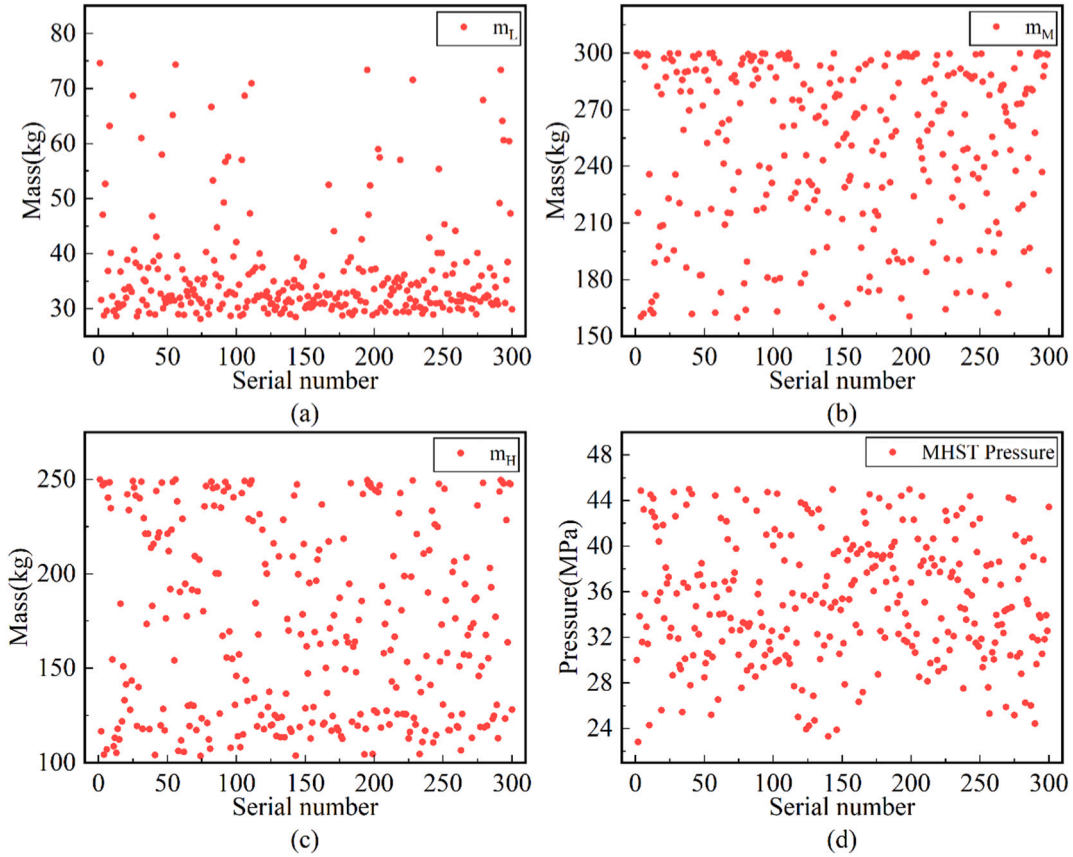

Fig. 9. Corresponding capacity and pressure of HST on the Pareto Front (a) LHST mass; (b) MHST mass; (c) HHST mass; (d) MHST pressure.

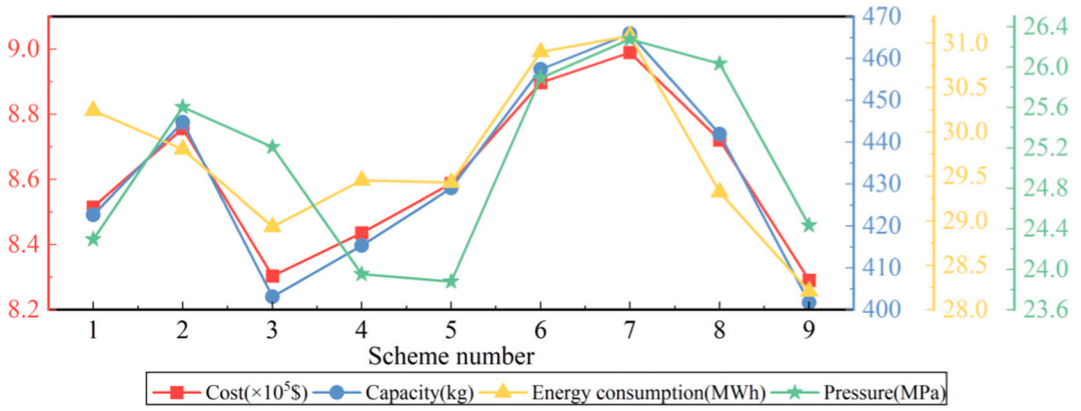

Fig. 10. Comparison of CHSS construction indicators for the selected schemes.

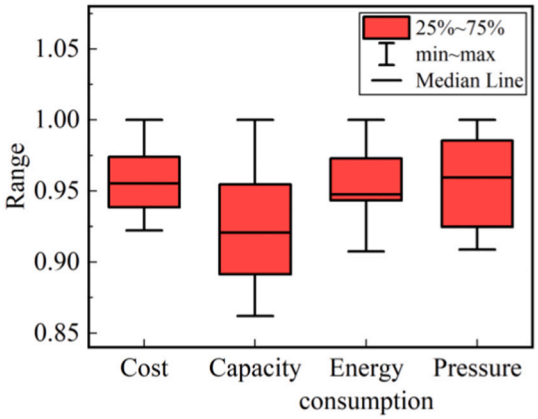

Fig. 11. Statistical results of the selected schemes.

distributed in the range between 22 and 40 MPa. It can be seen that there is not much difference in the unit energy consumption at different pressure levels in the search space. Therefore, the pressure is more uniformly distributed. As shown in Fig. 8, we selected 9 feasible solutions from the Pareto front that have lower compressor power consumption and total cost, while also having larger system capacity. Additionally, we numbered these 9 solutions according to the order calculated by NSGA-II. The year-long simulation results by applying the selected feasible solution to the park condition are shown in Fig. 10.

Based on the fluctuation range of cost, capacity, energy consumption, and pressure shown in Fig. 10, box plots are used to analyze their variation characteristics and determine the weights of the four indicators. Since the values of the four indicators vary significantly, the data are processed with each respective maximum value as the reference. The resulting analysis is presented as Fig. 11.

Table 5
Comprehensive evaluation of the schemes.

Scheme number	Cost (weight = 0.4)	Capacity (weight = 0.2)	Energy consumption (weight = 0.3)	Pressure (weight = 0.1)	Value
1	4	6	7	7	5.6
2	7	3	6	4	5.6
3	2	8	2	5	3.5
4	3	7	5	8	4.9
5	5	5	4	9	5.1
6	8	2	8	3	6.3
7	9	1	9	1	6.6
8	6	4	3	2	4.3
9	1	9	1	6	3.1

Among these four indicators, the cost is directly related to the economic efficiency of the system and exhibits the least volatility. Therefore, it is assigned a weight of 0.4 in the comprehensive evaluation. The larger the capacity, the stronger the system's load-bearing capacity, allowing it to accommodate and supply more hydrogen. However, capacity shows the greatest volatility among the four indicators, so its weight is set to 0.2 to reduce the impact of fluctuations on the accuracy of the results. Lower energy consumption indicates higher efficiency during system operation, which contributes to economic efficiency. Additionally, the pressure parameter is relatively more concentrated, so its weight is set to 0.3 in the comprehensive evaluation. Finally, higher pressure means the system occupies less space for the same capacity, so its weight is set to 0.1 in the comprehensive evaluation. Sorting the cost and energy consumption indexes of each scheme from small to large and the capacity and pressure from large to small, and calculating the final performance indicator I through equation.

$$I = \sum w_i R_i \tag{12}$$

where w_i is the weight of each indicator's ranking, and R_i is the magnitude of the ranking for each indicator. Table 5 can be obtained.

It can be seen that among the nine schemes with small differences in cost and energy consumption, although Scheme 7 has the largest capacity, it also has the highest cost and energy consumption, resulting in the worst composite index. In contrast, Scheme 9 has the smallest capacity, but it has the lowest cost and energy consumption, and highest pressure, so its comprehensive index is optimal. In summary, scheme 9 has the best performance and is the best intermediate pressure level and capacity configuration scheme.

After comparing the optimal capacity configuration of MHSS, the comparison with the two single-level schemes in Section 3 yields Fig. 12. It can be seen that the 45 MPa scheme is the largest and least economical

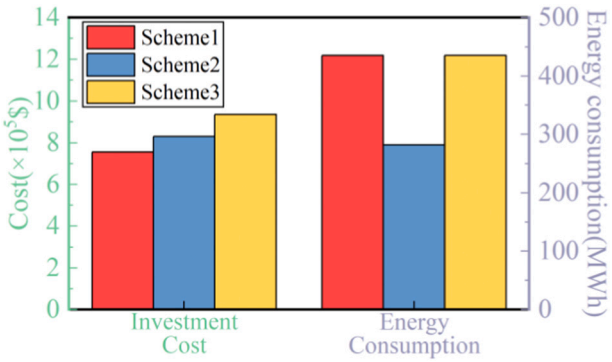

Fig. 12. Comparison of economic indicators for different schemes.

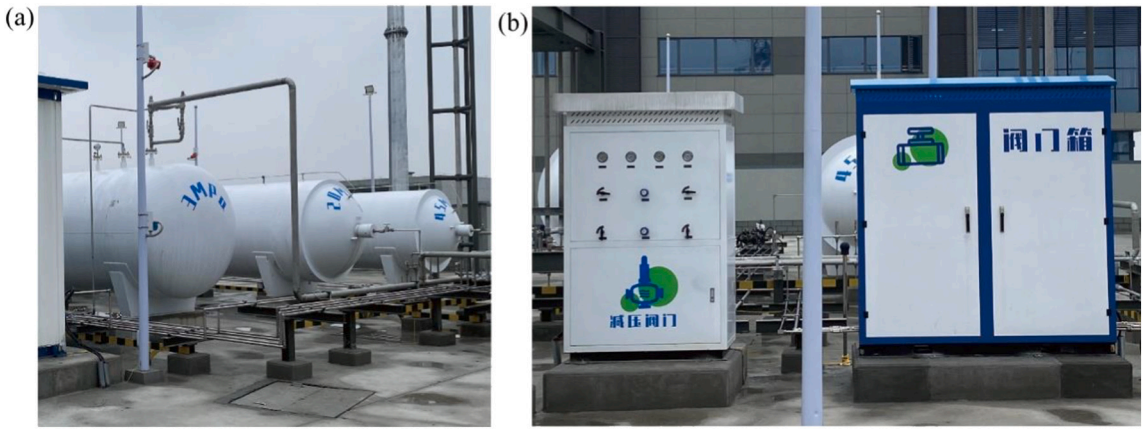

Fig. 13. Real park scene; (a) multilevel HSTs; (b) control valves.

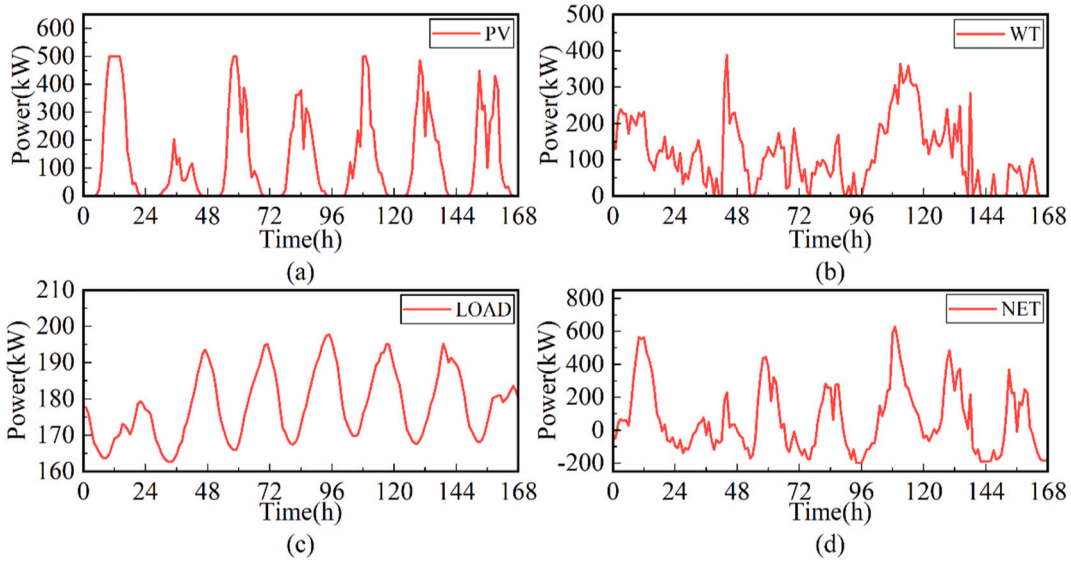

Fig. 14. Power curve (a) PV; (b) WT; (c) load; (d) net power.

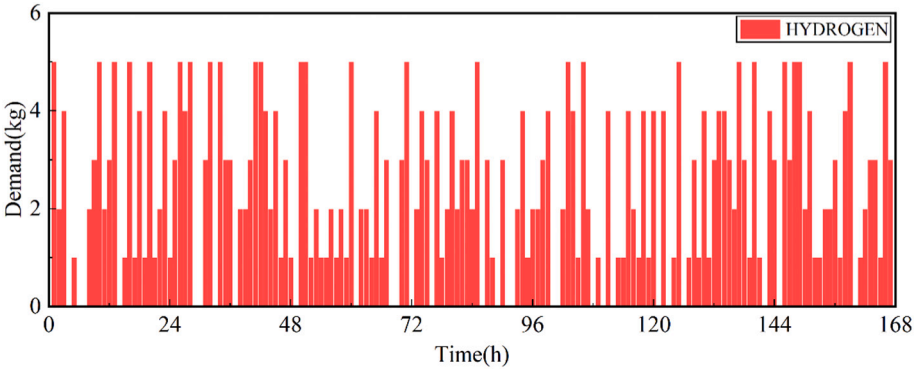

Fig. 15. Hydrogen loading curve (168 h).

in terms of both cost and energy consumption. The MHSS, on the other hand, increases costs by 9.7 % while reducing energy consumption by 35.19 % compared to the 3 MPa scheme, which makes the MHSS undoubtedly more economical in the long run.

4.2. *Typical scenario simulation*

The IHEUS involved in this study needs to operate in the off-grid mode for 168 h, and accordingly, the designed CHSS also faces the challenge of stable operation off-grid for 168 h. Based on the actual off-grid operation of 168 h in the demonstration park, as shown in Fig. 13, the optimal capacity configuration in Section 4.1 is further verified.

Table 6
System parameters.

	Capacity (kg)			Pressure (MPa)
	LHST	MHST	HHST	MHST
Actual system	40.19	267.9	200.93	20
Proposed system	30.82	257.84	113.04	24.44

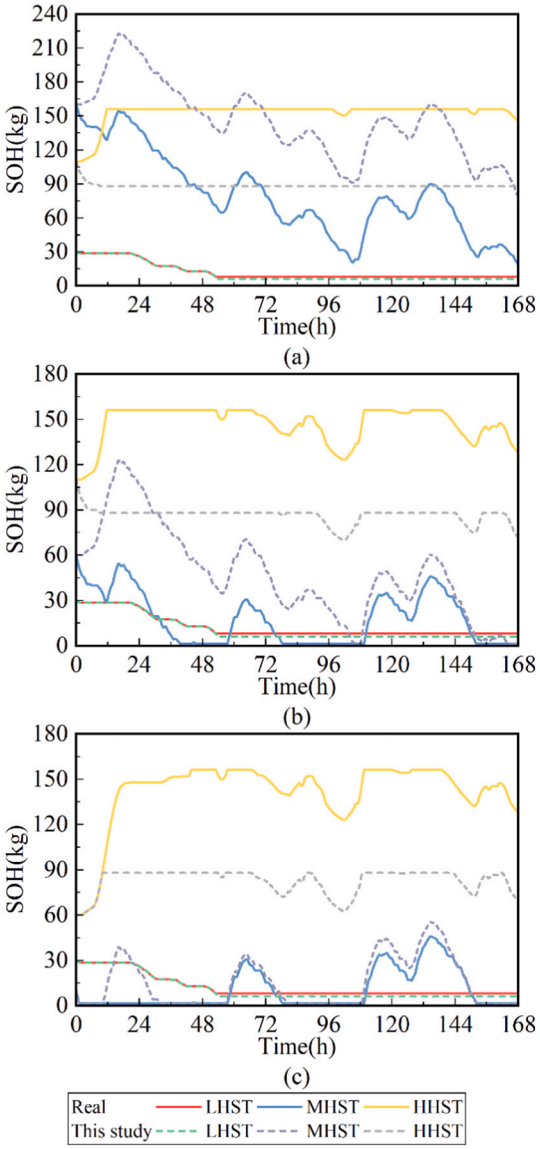

Fig. 16. SOH in different level HST. (a) Initial hydrogen storage capacity is 300 kg; (b) initial hydrogen storage capacity is 200 kg; (c) initial hydrogen storage capacity is 100 kg.

Table 7
The initial capacities of each HST.

Initial capacity (kg)	LHST	MHST	HHST
300	30	160	110
200	30	60	110
100	30	10	60

The source load curves of the 168 h off-grid operation test are shown in Figs. 14 and 15. The simulation verifies the optimized configuration, comparing it with the actual operating conditions experienced in the field over the same period and under similar climate conditions. The configurations of the actual system and the proposed system are shown in Table 6.

Fig. 16 illustrates the SOH curves obtained from simulating the operation of both the actual system and the optimized capacity determined in this study for 168 h. The simulation was conducted under identical source load conditions, with initial hydrogen capacities of 300 kg, 200 kg, and 100 kg for the CHSS, as detailed in Table 7. In Fig. 16, the solid lines are the data of the actual system, and the dashed line part is the system operation result designed in this study.

From Fig. 16, we observe that each HST operates effectively across the range of initial capacities. With an initial capacity of 300 kg, the MHSS boasts ample hydrogen storage, resulting in the HHST maintaining a consistently higher level of hydrogen with minimal fluctuations. Conversely, at an initial capacity of 200 kg, the HHST still sustains a high hydrogen level but experiences more pronounced fluctuations. At an initial capacity of 100 kg, however, the MHSS faces hydrogen shortages, making it challenging for the HHST to maintain stable hydrogen levels, resulting in significant fluctuations. Furthermore, the operating curves for HHSTs of the same level but different capacities exhibit similarities, with fluctuations correlating to the upper capacity limit. A higher capacity ceiling necessitates more hydrogen mass to maintain pressure, leading to greater SOH fluctuations.

Based on the off-grid 168 h operation, the MHSS at two capacities is evaluated by integrating five aspects: total capacity of the hydrogen storage system, the total energy consumption of the compressor within 168 h, total cost, MHST pressure magnitude and hydrogen supply loss rate (HSLR), obtaining Fig. 17 as shown. Where HSLR is the rate of the MHSS supplying insufficient hydrogen capacity, defined as the proportion of the hydrogen supply shortfall to the theoretical hydrogen supply. The calculation is as following equation

$$\mathrm{HSLR} = \frac{\text{Hydrogen supply loss}}{\text{Theoretical hydrogen supply}} \times 100\% \tag{13}$$

From Fig. 17, it's evident that the MHSS effectively meets hydrogen storage demands under both capacity configuration schemes when the initial capacity is set to 300 kg. However, there are shortages in hydrogen supply under other initial capacity conditions. The scheme proposed in this study reduces HSLR by 11.64 % and 12.13 % at initial capacities of 200 kg and 100 kg, respectively. Notably, when the initial capacity is set to 300 kg, the hydrogen initial capacity is sufficient, and with a larger capacity, it avoids overloading HST, thereby causing the compressor to operate for long periods, resulting in lower energy consumption of the compressor in the actual capacity configuration scheme compared to the scheme designed in this study. However, in all other initial capacity conditions, the energy consumption of the capacity configuration scheme designed in this study is lower. Additionally, compared with the field configuration scheme, the scheme designed in this study reduces costs by approximately $17,000, and the MHST pressure increases by about 4.4 MPa. Consequently, the load capacity of the MHSS is reduced by about 100 kg. In summary, the capacity configuration scheme designed in this study outperforms the actual scheme under the test conditions.

5. Conclusion

In this study, a cascade hydrogen storage system (CHSS) for integrated hydrogen energy utilization is proposed using multiple pressure levels. Firstly, a mathematical model and an economic model of the CHSS are established. By comparing the economics of different structures of the cascade system, the design of the system is determined. A hydrogen scheduling strategy is proposed to improve the response speed and stability of the system. Secondly, the cascaded structure is compared with the conventional design with the single pressure level for supporting a 168-h off-grid operation. The results verify the feasibility of the proposed system and the optimization algorithm. The main concluding

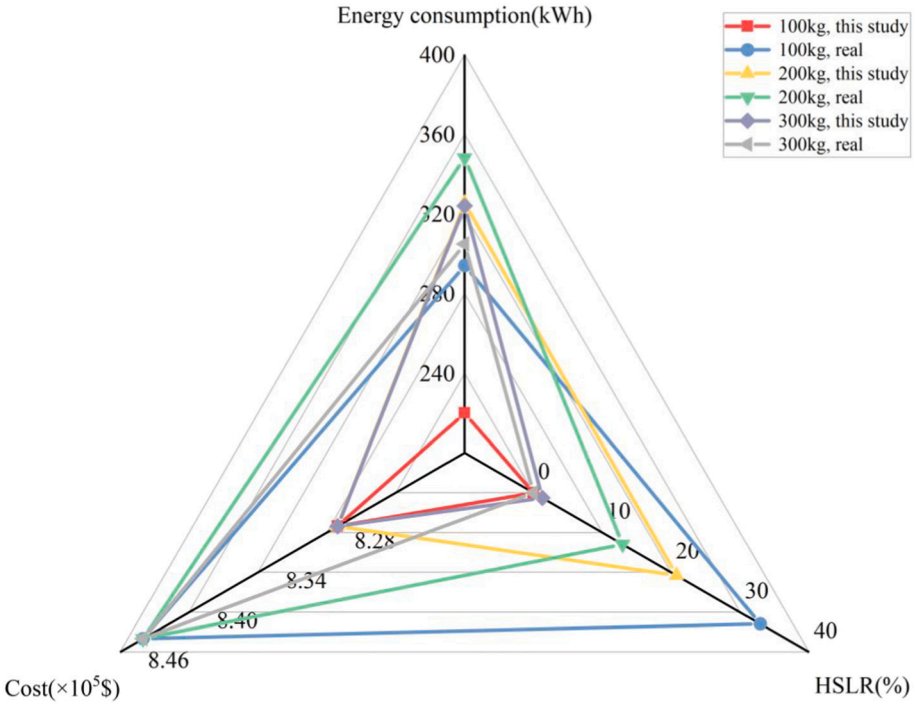

Fig. 17. Comparative diagram of three hydrogen storage schemes.

remarks are as follows:

1) The proposed CHSS is applicable to IHEUS for storing hydrogen produced by a hydrogen production system in three pressure levels, i.e., 3 MPa, 24.44 MPa, and 45 MPa, which are used for supplying hydrogen to a power generation system, long-term storage of hydrogen, and supplying hydrogen to a hydrogen refueling station, respectively, and to design a corresponding hydrogen management strategy to improve the stability of the system.
2) Using the established economic model, the comparative analysis shows that the cascaded system can reduce 35.19 % of the energy consumption compared to the single-level low-pressure system, and 11.43 % of cost reduction is offered compared to the single-level high-pressure system.
3) NSGA-II is used to optimize the system capacity configuration, and the optimal configuration results are obtained by weighted calculation combined with the actual engineering. The simulated system is operated under off-grid 168 h conditions. Compared with the actual capacity configuration scheme, the overall cost is reduced by 2.01 %, the energy consumption during operation is reduced by about 6.92 %, and HSLR is reduced by about 12 %.

CRediT authorship contribution statement

Shihao Zhu: Writing – original draft, Investigation, Formal analysis, Data curation. **Banghua Du:** Software, Methodology. **Xinyu Lu:** Investigation, Data curation. **Changjun Xie:** Writing – review & editing, Supervision, Funding acquisition, Conceptualization. **Yang Li:** Writing – review & editing, Visualization. **Yunhui Huang:** Resources, Methodology. **Leiqi Zhang:** Validation, Project administration. **Bo Zhao:** Resources, Project administration.

Declaration of competing interest

The authors declare that they have no known competing financial interests or personal relationships that could have appeared to influence the work reported in this paper.

Data availability

Data will be made available on request.

Acknowledgements

This paper is supported by the National Key Research and Development Program of China (No. 2020YFB1506802).

References

[1] Y. Qiu, T. Zeng, C. Zhang, G. Wang, Y. Wang, Z. Hu, Z. Wei, Progress and challenges in multi-stack fuel cell system for high power applications: architecture and energy management, Green Energy and Intelligent Transportation 2 (2) (2023) 100068.
[2] X. Lu, B. Du, W. Zhu, Y. Yang, C. Xie, Z. Tu, Z. Deng, Thermodynamic and dynamic analysis of a hybrid PEMFC-ORC combined heat and power (CHP) system, Energy Convers. Manag. 292 (2023) 117408.
[3] X. Xu, Q. Zhou, D. Yu, The future of hydrogen energy: bio-hydrogen production technology, Int. J. Hydrog. Energy 47 (79) (2022) 33677–33698.
[4] X. Lu, B. Du, S. Zhou, W. Zhu, Y. Li, Y. Yang, Z. Deng, Optimization of power allocation for wind-hydrogen system multi-stack PEM water electrolyzer considering degradation conditions, Int. J. Hydrog. Energy 48 (15) (2023) 5850–5872.
[5] H. Zhang, Y. Chen, K. Liu, S. Dehan, A novel power system scheduling based on hydrogen-based micro energy hub, Energy 251 (2022) 123623.
[6] Z. Abdin, K. Khalilpour, K. Catchpole, Projecting the levelized cost of large scale hydrogen storage for stationary applications, Energy Convers. Manag. 270 (2022) 116241.
[7] A.M. Elberry, J. Thakur, A. Santasalo-Aarnio, M. Larmi, Large-scale compressed hydrogen storage as part of renewable electricity storage systems, Int. J. Hydrog. Energy 46 (29) (2021) 15671–15690.
[8] P. Jena, Materials for hydrogen storage: past, present, and future, The Journal of Physical Chemistry Letters 2 (3) (2011) 206–211.
[9] M.G. Rasul, M.A. Hazrat, M.A. Sattar, M.I. Jahirul, M.J. Shearer, The future of hydrogen: challenges on production, storage and applications, Energy Convers. Manag. 272 (2022) 116326.
[10] I.A. Hassan, H.S. Ramadan, M.A. Saleh, D. Hissel, Hydrogen storage technologies for stationary and mobile applications: review, analysis and perspectives, Renew. Sust. Energ. Rev. 149 (2021) 111311.
[11] B. Sorensen, Hydrogen and Fuel Cells: Emerging Technologies and Applications, 2011.
[12] T. Zhang, J. Uratani, Y. Huang, L. Xu, S. Griffiths, Y. Ding, Hydrogen liquefaction and storage: recent progress and perspectives, Renew. Sust. Energ. Rev. 176 (2023) 113204.

[13] J. Ren, N.M. Musyoka, H.W. Langmi, M. Mathe, S. Liao, Current research trends and perspectives on materials-based hydrogen storage solutions: a critical review, Int. J. Hydrog. Energy 42 (1) (2017) 289–311.
[14] I.P. Jain, C. Lal, A. Jain, Hydrogen storage in mg: a most promising material, Int. J. Hydrog. Energy 35 (10) (2010) 5133–5144.
[15] Z. Yanxing, G. Maoqiong, Z. Yuan, D. Xueqiang, S. Jun, Thermodynamics analysis of hydrogen storage based on compressed gaseous hydrogen, liquid hydrogen and cryo-compressed hydrogen, Int. J. Hydrog. Energy 44 (31) (2019) 16833–16840.
[16] M.R. Usman, Hydrogen storage methods: review and current status, Renew. Sust. Energ. Rev. 167 (2022) 112743.
[17] Ł. Bartela, A hybrid energy storage system using compressed air and hydrogen as the energy carrier, Energy 196 (2020) 117088.
[18] Y. Zhang, Q.S. Hua, L. Sun, Q. Liu, Life cycle optimization of renewable energy systems configuration with hybrid battery/hydrogen storage: a comparative study, Journal of Energy Storage 30 (2020) 101470.
[19] M.R. Maghami, R. Hassani, C. Gomes, H. Hizam, M.L. Othman, M. Behmanesh, Hybrid energy management with respect to a hydrogen energy system and demand response, Int. J. Hydrog. Energy 45 (3) (2020) 1499–1509.
[20] S. Basu, A. John, A. Kumar, Design and feasibility analysis of hydrogen based hybrid energy system: a case study, Int. J. Hydrog. Energy 46 (70) (2021) 34574–34586.
[21] Y. Song, H. Mu, N. Li, X. Shi, X. Zhao, C. Chen, H. Wang, Techno-economic analysis of a hybrid energy system for CCHP and hydrogen production based on solar energy, Int. J. Hydrog. Energy 47 (58) (2022) 24533–24547.
[22] Z. Abdin, W. Mérida, Hybrid energy systems for off-grid power supply and hydrogen production based on renewable energy: a techno-economic analysis, Energy Convers. Manag. 196 (2019) 1068–1079.
[23] H. Dong, Z. Shan, J. Zhou, C. Xu, W. Chen, Refined modeling and co-optimization of electric-hydrogen-thermal-gas integrated energy system with hybrid energy storage, Appl. Energy 351 (2023) 121834.
[24] M. Li, Y. Bai, C. Zhang, Y. Song, S. Jiang, D. Grouset, M. Zhang, Review on the research of hydrogen storage system fast refueling in fuel cell vehicle, Int. J. Hydrog. Energy 44 (21) (2019) 10677–10693.
[25] C. Tarhan, M.A. Çil, A study on hydrogen, the clean energy of the future: hydrogen storage methods, Journal of Energy Storage 40 (2021) 102676.
[26] T. Mayer, M. Semmel, M.A.G. Morales, K.M. Schmidt, A. Bauer, J. Wind, Techno-economic evaluation of hydrogen refueling stations with liquid or gaseous stored hydrogen, Int. J. Hydrog. Energy 44 (47) (2019) 25809–25833.
[27] P. Fragiacomo, M. Genovese, Numerical simulations of the energy performance of a PEM water electrolysis based high-pressure hydrogen refueling station, Int. J. Hydrog. Energy 45 (51) (2020) 27457–27470.
[28] S.E. Ahmadi, D. Sadeghi, M. Marzband, A. Abusorrah, K. Sedraoui, Decentralized bi-level stochastic optimization approach for multi-agent multi-energy networked micro-grids with multi-energy storage technologies, Energy 245 (2022) 123223.
[29] L. Hu, Q. Tian, C. Zou, J. Huang, Y. Ye, X. Wu, A study on energy distribution strategy of electric vehicle hybrid energy storage system considering driving style based on real urban driving data, Renew. Sust. Energ. Rev. 162 (2022) 112416.
[30] C. Xu, Y. Ke, Y. Li, H. Chu, Y. Wu, Data-driven configuration optimization of an off-grid wind/PV/hydrogen system based on modified NSGA-II and CRITIC-TOPSIS, Energy Convers. Manag. 215 (2020) 112892.
[31] G. Pan, W. Gu, Y. Lu, H. Qiu, S. Lu, S. Yao, Optimal planning for electricity-hydrogen integrated energy system considering power to hydrogen and heat and seasonal storage, IEEE Transactions on Sustainable Energy 11 (4) (2020) 2662–2676.
[32] B. Du, S. Zhu, W. Zhu, X. Lu, Y. Li, C. Xie, J. Song, Energy management and performance analysis of an off-grid integrated hydrogen energy utilization system, Energy Convers. Manag. 299 (2024) 117871.
[33] G. Liu, Y. Qin, J. Wang, C. Liu, Y. Yin, J. Zhao, O.N. Otoo, Thermodynamic modeling and analysis of a novel PEMFC-ORC combined power system, Energy Convers. Manag. 217 (2020) 112998.
[34] Y. Zhou, Y. Li, W. Gao, Experimental investigation on the effect of a barrier wall on unconfined hydrogen explosion, Int. J. Hydrog. Energy 48 (86) (2023) 33763–33773.
[35] Henan Yuqing Hydrogen Equipment Co., Ltd. (n.d.). Hydrogen compressor. Retrieved from http://www.hnyqzb.com/proinfo/17.html.
[36] E. Haghi, M. Fwoler, K. Raahemifar, Economic analysis of hydrogen production in context of a microgrid, in: 2017 IEEE International Conference on Smart Energy Grid Engineering (SEGE), IEEE, August 2017, pp. 79–84.
[37] Zhejiang Juhua Co., Ltd. (n.d.). Zhejiang Juhua Co., Ltd. Retrieved from http://www.jhgf.com.cn.
[38] R. Saidur, N.A. Rahim, M. Hasanuzzaman, A review on compressed-air energy use and energy savings, Renew. Sust. Energ. Rev. 14 (4) (2010) 1135–1153.
[39] X. Lü, Y. Wu, J. Lian, Y. Zhang, C. Chen, P. Wang, L. Meng, Energy management of hybrid electric vehicles: a review of energy optimization of fuel cell hybrid power system based on genetic algorithm, Energy Convers. Manag. 205 (2020) 112474.
[40] H. Liu, Y. Li, Z. Duan, C. Chen, A review on multi-objective optimization framework in wind energy forecasting techniques and applications, Energy Convers. Manag. 224 (2020) 113324.